IEEE Access
Multidisciplinary | Rapid Review | Open Access Journal

Received November 19, 2018, accepted December 4, 2018, date of publication December 10, 2018,
date of current version January 7, 2019.

Digital Object Identifier 10.1109/ACCESS.2018.2886041

From Threads to Smart Textile: Parametric Characterization and Electromagnetic Analysis of Woven Structures

LETICIA ALONSO-GONZÁLEZ, (Member, IEEE), SAMUEL VER-HOEYE, (Member, IEEE), MIGUEL FERNÁNDEZ-GARCÍA, CARLOS VÁZQUEZ-ANTUÑA, AND FERNANDO LAS-HERAS ANDRÉS, (Senior Member, IEEE)

Área de Teoría de la Señal y Comunicaciones, Departamento de Ingeniería Eléctrica, Universidad de Oviedo, 33203 Gijón, Spain

Corresponding author: Leticia Alonso-González (alonsoleticia@uniovi.es)

This work was supported in part by the Spanish Agencia Estatal de Investigación (AEI) and Fondo Europeo de Desarrollo Regional (FEDER) under Project TEC2016-80815-P (AEI/FEDER-UE), Project TEC2015-72110-EXP (AEI), and Grant FPU14/00016, and in part by the Gobierno del Principado de Asturias (PCTI/FEDER-FSE) under Project IDI/2016/000372 and Project IDI/2017/000083.

ABSTRACT This paper presents a complete and enhanced description of a parametric characterization and an electromagnetic analysis technique in order to simulate complex woven structures for the design of wearable microwave circuits and antennas based on smart textile. On the one hand, the parametric characterization consists of achieving the mathematical models which describe the different patterns conformed by the threads of the woven structures. This characterization takes into account the possible deformations of the materials inside the woven structure. On the other hand, the electromagnetic analysis technique consists of studying the conductive or dielectric parameters which describe the materials from which the threads have been extruded, and predicting the electromagnetic behavior of whole woven structures using the already explained parametric characterization. For this purpose, three different, although electromagnetically equivalent, models of the involved materials are needed, which subsequently reduce the computational resources required in the simulations. As a result, the woven structures can be characterized from the involved threads and the electromagnetic behavior can be analyzed in order to design wearable antennas or circuits.

INDEX TERMS Antennas, circuits, electromagnetic analysis, microwave, modeling technique, multifilament yarns, simulations, skin effect, smart textile, threads, woven structures.

I. INTRODUCTION

New approaches in the development of textile circuits and antennas are continually emerging to cope with the advances in flexible, lightweight and wearable applications [1], [2]. Therefore, multiple efforts are being made to achieve the full integration of these circuits and antennas in textile. Consequently, during the last years, a wide variety of solutions have been developed to design and manufacture textile integrated circuits and antennas. In the following paragraphs, a brief overview of the state-of-the-art in textile integration techniques is presented.

Ink-jet printing is a type of computerized printing which consists of recreating a pattern by propelling droplets of ink onto different substrates and a posterior curing process. Silver nanoparticles can be used for highly conductive inks, whereas carbon nanotube inks are employed for applications where the conductivity can be lower. This technique has been directly employed over substrates [3]–[9] to develop RF circuits and antennas, although it can be enhanced by printing over an impermeable coated intermediate layer [10], [11] or printing multiple stacked conductive layers [12]. Although this technique presents the advantage of achieving complex details in the designs, the requirement of interface or additional layers supposes time during the manufacturing process. Besides, the impossibility of developing multilayered prototypes reduces the variety of implementable designs.

Embroidery is the art of realize patterns by means of stitches sewn directly onto an existing fabric. The patterns can be embroidered using electrically conductive threads, which provide a wide range of alternatives to develop RF circuits and antennas. Conductive embroidered lines can be employed to develop contour antennas [13] or manufacturing

rows of conductive vias for existing circuits [14], whereas conductive meshes can be used for planar circuits [15]–[18]. This technique allows the achievement of complex designs due to the high resolution provided by the stitches. Nevertheless, in spite of the fact that embroidering does not allow the realization of different patterns in both sides of an existing fabric, two individually embroidered fabrics can be employed and subsequently connected [19].

Applique processes consist of attaching various textile materials employing different alternatives leading to a wide variety of designs to develop RF circuits and antennas. Different materials can be employed to implement both the conductive elements and the dielectric substrates of the circuits and antennas [20]–[25]. In order to attach the textile materials, sewing procedures [20], [23], [26], adhesives [21], or eyelets [22] can be employed. Applique processes present various advantages due to the fact that using different separate structured layers allows multilayered prototypes [22], [25], [26]. Nevertheless, these techniques require several subprocesses to develop a final prototype, leading to a non-fully textile integrated circuit or antenna.

Non-wovens are fabric-like materials made from short staple fibers and continuous long fibers, bonded together by different treatments, leading to materials which are neither woven nor knitted. Non-wovens typically lack strength unless densified or reinforced. A non-woven itself is not a technique, but a material. However, non-wovens together with one of the previously presented techniques, can lead to the design of textile RF circuits or antennas. Different materials can be employed as both conductive [27]–[31] or dielectric [32] non-woven fabrics. As advantages, non-wovens provide higher levels of uniformity and consistency to high temperatures. However, one or more of the before mentioned techniques must be applied.

In spite of the wide range of approaches presented in the previous paragraphs, none of these techniques can produce, simultaneously, multilayered, completely textile-integrated and available for large-scale production prototypes. For this reason and with the aim of fulfilling these requirements, weaving technology is employed in this work. In order to develop and electromagnetically study complex woven antennas and circuits, a parametric characterization and corresponding analysis are required due to the difficulty of working with woven structures. As a consequence, a first approach to study the behavior of conductive threads has already been introduced in [33]. Additionally, the authors have previously presented some partial results of the characterization and analysis of woven structures using simplified procedures in [34]–[38]. Finally, in this paper, a complete and enhanced parametric characterization and corresponding electromagnetic analysis are presented and validated using different examples.

This paper is organized as follows. In Section II, the three-step modeling to characterize woven structures is introduced. In Section III, the filament model is thoroughly explained. In Section IV, the monofilament model is analyzed and the translation from the filament model to the monofilament model is explained. In Section V, the layers model is presented and the corresponding translation from the monofilament model is analyzed. In Section VI, different examples of use are presented for the validation of the characterization and analysis. Finally, conclusions are drawn.

II. DESCRIPTION OF THE THREE-STEP MODELLING

In order to achieve a woven structure, two different kinds of threads can be employed, monofilament or multifilament threads. The monofilament threads are easier to analyze, although they lack flexibility. For this reason, the woven structures are normally manufactured using multifilament threads, which are more flexible. Additionally, the threads which compose a woven structure can be divided into two categories, the warp threads and the weft threads. The warp threads, which are parallel to the warp direction, are previously assembled in the loom, whereas the weft threads–which are parallel to the weft direction–are successively inserted in the woven structure during the fabrication process. The herein presented technique is a parametric characterization of the textile materials required to compose a complex and multilayered woven structure.

First, the materials from which the threads have been extruded need to be analyzed, whether they are electrically conductive or dielectric. For this purpose, the filament model (FM) is employed. Secondly, the multifilament threads are translated into electromagnetically equivalent and simpler monofilament threads thanks to the monofilament model (MM). Once the equivalent monofilaments are achieved, a mathematical model of the paths corresponding to the threads must be worked out. This model takes into account the possible deformations of the woven structure due to the forces actuating between the threads. Finally, the MM can be translated into the simplest model, the layers model (LM), which emulates the conventional procedure to simulate circuits or antennas, using homogeneous materials.

In order to work out the electromagnetic analysis of the whole woven structure, each of the beforementioned models must be studied. For the dielectric materials, a procedure based on a rectangular waveguide can be used in order to translate from the FM to the MM, and from the MM to the LM, which will be then explained in detail. Nevertheless, when analyzing the conductive materials, the procedure is more complicated, as the skin effect associated to the conductive filaments which compose the multifilament threads must be taken into account, in order to translate from the FM to the LM. As with the dielectrics, the waveguide procedure can then be used to translate from the MM to the LM. The different modeling steps and the most important parameters required to translate between the different modelings are summarized in Figure 1 and will be described in detail in the following sections. Using this modeling, a woven structure can be electromagnetically analyzed before its fabrication.

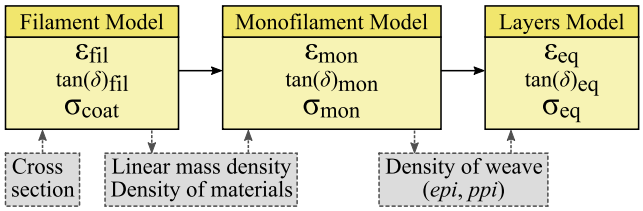

FIGURE 1. Three-step characterization model, corresponding relative permittivities, loss tangents and electrical conductivities and required parameters for translation between models.

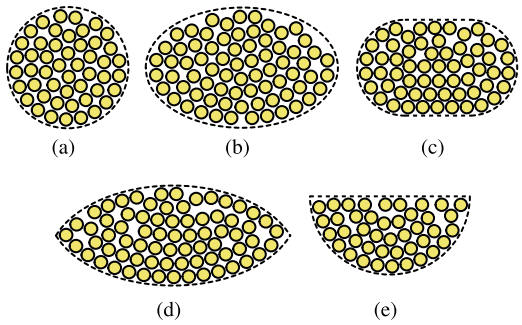

FIGURE 2. Different distributions of the filaments in the cross section of a multifilament thread. (a) Circular. (b) Pierce's elliptic. (c) Kemp's racetrack. (d) Hearle. (e) Bowshaped.

III. FILAMENT MODEL

The FM emulates the real composition of the thread and represents the most computationally complex problem. It takes into account the number of filaments which compose the thread, the dimensions of each filament and the characteristic parameters of the material from which the filaments have been extruded, which are the relative dielectric permittivity, ϵ_{fil}, and the loss tangent, $\tan(\delta)_{\text{fil}}$, for the dielectric yarns, or the conductivity of the coating, σ_{coat}, for the electrically conductive threads.

During the fabrication process of the multifilament threads, the different filaments tend to be packed adopting a circularly-shaped cross section, as generically depicted in Figure 2a. However, this cross section tends to deform when the threads are in a woven structure, due to the forces they experiment. Some approaches to characterize the deformed cross section of these threads have been widely used such as the Pierce's elliptic cross section (Figure 2b), the Kemp's racetrack section (Figure 2c), the Hearle's section (Figure 2d) or the Bowshaped geometry (Figure 2e) [39]. The corresponding dimensions to characterize the different cross sections are summarized in Figure 3.

As a consequence, using the FM, the distribution of the filaments which compose the complete multifilament yarn can be analyzed and approximated by one of the possibilities presented in Figure 2. Normally, the procedure to analyze these cross sections is empirical and is based on the observation of different samples of the yarns under a microscope.

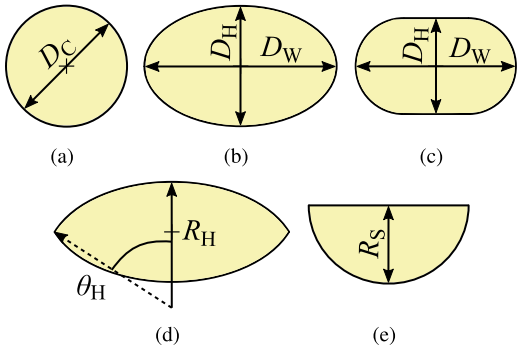

FIGURE 3. Dimensions of the cross sections for the different distributions of the filaments in a multifilament thread. (a) Circular. (b) Pierce's elliptic. (c) Kemp's racetrack. (d) Hearle. (e) Bowshaped.

IV. MONOFILAMENT MODEL

The MM represents an electromagnetically equivalent textile structure by replacing the multifilament threads with monofilament threads, and reducing the computational complexity. Depending on the electromagnetic behavior of the thread, electrically conductive or dielectric, a different procedure to translate from the FM to the MM is required. This model is then used to create the complete parametric woven structure, which is formed using the mathematical expressions of the paths corresponding to the different threads.

A. DIELECTRIC MATERIALS

Due to the air gaps between the filaments that are forming the thread, the relative permittivity of its equivalent dielectric monofilament is reduced and denoted by ϵ_{mon}. Correspondingly, a new loss tangent can be defined and denoted by $\tan(\delta)_{\text{mon}}$.

To translate the FM into the MM, a theoretical method has been used. For this purpose, the linear mass density of the thread, L_{dtex}, the density of the material from which the filaments have been extruded, δ_{fil}, and the geometric parameters of the thread (cross section dimensions and length: W, H and L, respectively, as depicted in Figure 4a) must be taken into account. The linear mass density of the threads is commonly measured using the dtex unit.

Given a generic thread with an elliptic cross section, its volume is given by $V_o = \pi WHL/2$. The linear mass density per unit length represents the weight of the thread per unit length, including the air gaps. If it is specified using dtex, then it is defined for $L = 10$ Km. The density parameter represents the weight of the material per unit volume. Therefore, given a thread whose volume is V_o, if the value of its linear mass density is compared to the value of its weight, the proportion of air inside the thread can be calculated as summarized in Figure 4a.

Simulating a rectangular waveguide which has been filled with filaments (ϵ_{fil} and $\tan(\delta)_{\text{fil}}$), using the same proportion of air as there is inside the thread, and comparing its electromagnetic behavior with another rectangular waveguide which has been homogeneously filled, the corresponding

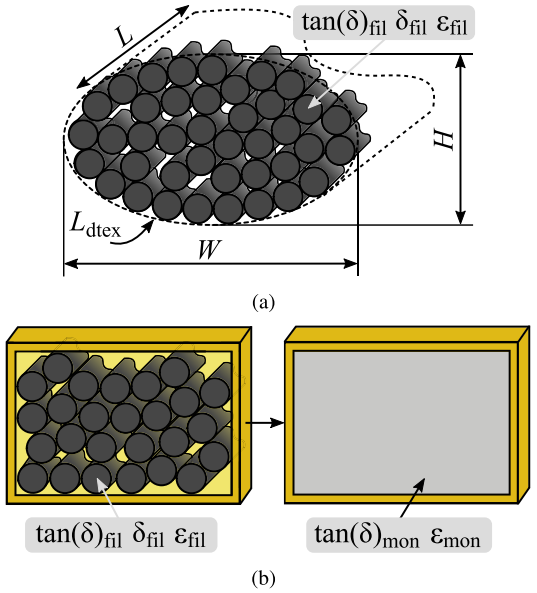

FIGURE 4. Translation from FM to MM. (a) Parameters involved in the translation from the FM into the MM using dielectric materials. (b) Overview of the waveguide procedure.

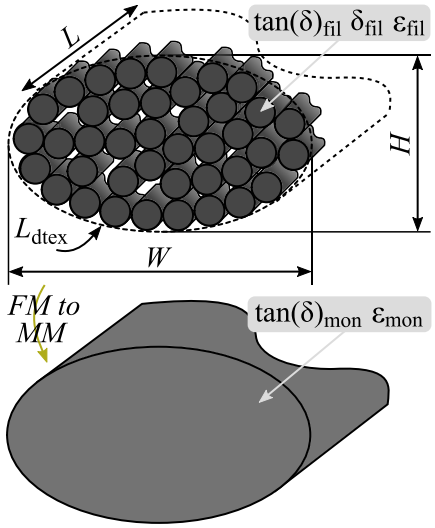

FIGURE 5. Translation from the FM into the MM outline applied to dielectric threads.

ϵ_{mon} and $\tan(\delta)_{\text{mon}}$ parameters can be easily extracted from the cut-off frequency and the insertion losses as summarized in Figure 4b. Therefore, a dielectric multifilament thread can be translated into its equivalent monofilament thread as depicted in Figure 5. As this new monofilament thread represents an homogeneous material, the computational complexity of its corresponding electromagnetic simulation is dramatically reduced.

B. CONDUCTIVE MATERIALS

The study of the conductive multifilament threads requires a more thorough analysis. Conductive threads can be

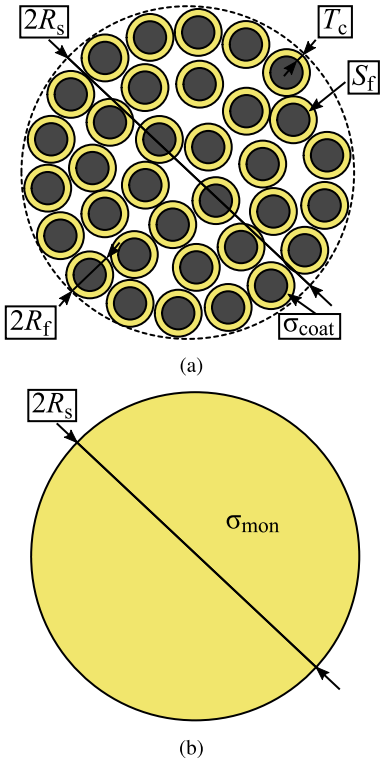

FIGURE 6. Translation from a conductive multifilament thread into a conductive monofilament thread. (a) Conductive multifilament thread cross section. (b) Equivalent conductive monofilament thread cross section.

manufactured from a conductive material, or can be made from dielectric materials and subsequently coated with conductive material. The coating procedure includes three steps. First, the non-coated threads are knitted into a fabric. Secondly, the fabric is plated with the conductive material by an electrolysis process. Finally, the fabric is de-knitted and it can be guaranteed that every thread has been completely plated. Consequently, the thickness of the coating and its composition become relevant, then, the skin effect has to be analyzed.

Figure 6a depicts an example of a multifilament thread, whereas Figure 6b represents its electromagnetically equivalent monofilaments. The aim of this section is to calculate the electrical conductivity of the equivalent monofilament, σ_{mon}, applied to a circular cross section, for simplicity. Nevertheless, this methodology can be extended to the rest of the already mentioned cross sections.

The skin depth can be calculated from the expression (1), where δ is the skin effect depth, ρ_{coat} is the resistivity of the material employed for the coating, f is the operating frequency and μ is the magnetic permeability. The first step in the characterization of the conductive materials is the comparison between the calculated skin depth, δ, and the thickness of the conductive coating which has been applied to each filament, T_c. Two different procedures have to be taken into account to translate the multifilament thread into its analogous monofilament, depending on the fact that the

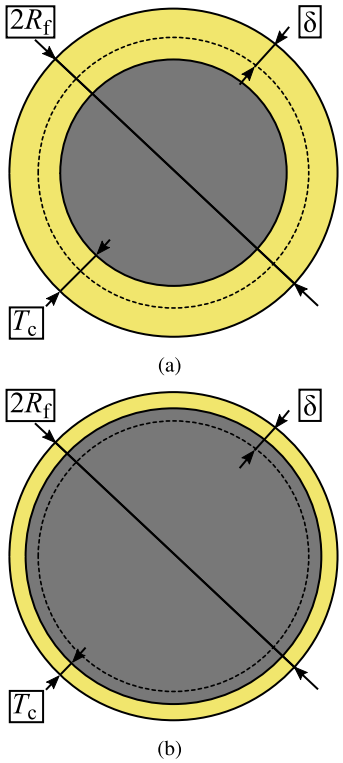

FIGURE 7. Different cases in the translation from the multifilament thread into the analogous monofilament thread, using the magnification of a single filament. (a) $\delta \leq T_c$. (b) $\delta > T_c$.

skin depth is less or equal, or greater than the thickness of the conductive coating applied to each filament. Both cases are schematically represented in Figure 7.

$$\delta = \sqrt{\frac{\rho_{coat}}{\pi f \mu}} \tag{1}$$

1) THE SKIN DEPTH IS LESS OR EQUAL THAN THE THICKNESS OF THE CONDUCTIVE COATING

If the skin depth is less or equal than the thickness of the conductive coating applied to each filament, $\delta \leq T_c$, the resistance per unit length of each filament can be calculated using (2), where $(R/l)_f$ denotes the resistance per unit length of each filament, ρ_{coat} and σ_{coat} are, respectively, the resistivity and conductivity of the material employed for the coating, and S_f represents the area of the effective conductive cross section of each filament.

$$(R/l)_f = \frac{\rho_{coat}}{S_f} = \frac{1}{\sigma_{coat} \cdot S_f} \tag{2}$$

In order to calculate the effective conductive cross section of each filament, as the δ is less or equal than T_c, the δ parameter has to be taken into account instead of T_c. Consequently, the S_f associated to a single filament whose external radius (including the coating) is R_f is given by (3).

$$S_f = \pi \cdot R_f^2 - \pi \cdot (R_f - \delta)^2 = \pi \cdot (2 \cdot R_f \cdot \delta - \delta^2) \tag{3}$$

Substituting (3) in (2), the resistance per unit length of a single filament is given by (4). Consequently, the resistance per unit length of a multifilament thread, (R/l), composed of N_{fil} filaments is given by (5).

$$(R/l)_f = \frac{1}{\sigma_{coat} \cdot \pi \cdot (2 \cdot R_f \cdot \delta - \delta^2)} \tag{4}$$

$$(R/l) = \frac{(R/l)_f}{N_{fil}} = \frac{1}{N_{fil} \cdot \sigma_{coat} \cdot \pi \cdot (2 \cdot R_f \cdot \delta - \delta^2)} \tag{5}$$

With the aim of substituting the multifilament thread by an electromagnetically equivalent monofilament thread, the effective radius of the multifilament thread, R_S, must be taken into account. Therefore, the electromagnetically equivalent monofilament thread must have the same radius, R_S, in order to keep the same woven structure.

The monofilament thread is provided with a conductive coating (σ_{mon}) whose thickness is given by T_R, leading to a corresponding area of the conductive cross section denoted by S_{mon}. The S_{mon} can be calculated using (6).

$$S_{mon} = \pi \cdot R_S^2 - \pi \cdot (R_S - T_R)^2 = \pi \cdot (2 \cdot R_S \cdot T_R - T_R^2) \tag{6}$$

In order to guarantee the electromagnetic equivalence between the multifilament thread and the proposed monofilament thread, the resistances per unit length must be the identical. For this purpose, the resistance per unit length of the monofilament thread, $(R/l)_{mon}$, can be calculated using (7). Alternatively, the resistance per unit length of the multifilament thread, (R/l), has been previously calculated in (5).

$$(R/l)_{mon} = \frac{1}{\sigma_{mon} \cdot \pi \cdot (2 \cdot R_S \cdot T_R - T_R^2)} \tag{7}$$

The condition of achieving the same resistance per unit length with both threads, leads to the equation presented in (8).

$$\frac{1}{\sigma_{mon} \cdot (2 \cdot R_S \cdot T_R - T_R^2)} = \frac{1}{N_{fil} \cdot \sigma_{coat} \cdot (2 \cdot R_f \cdot \delta - \delta^2)} \tag{8}$$

Nevertheless, the electromagnetic field penetrates a distance given by the skin depth in the monofilament, therefore, it must be calculated. The skin depth in the monofilament thread is denoted by δ_{mon} and can be calculated using (9). Consequently, $T_R = \delta_{mon}$.

$$\delta_{mon} = \sqrt{\frac{1}{\sigma_{mon} \pi f \mu}} \tag{9}$$

Substituting the expressions (1) and (9) in (8) and simplifying, the value of the electrical conductivity of the equivalent monofilament, σ_{mon}, can be calculated using (10), where σ_{mon} depends on the cross section of the equivalent monofilament (R_S), the frequency (f), the number of filaments which compose each multifilament thread (N_{fil}), the magnetic permeability (μ) and the electrical conductivity of the

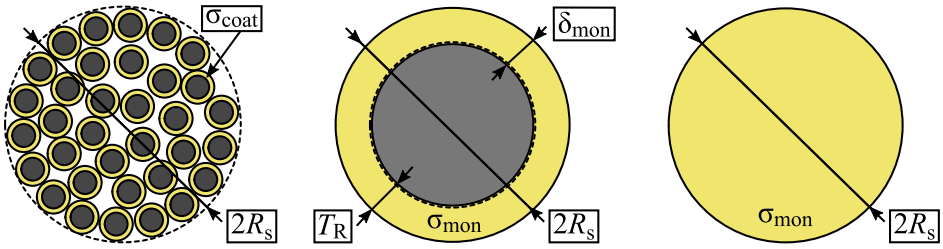

FIGURE 8. Translation from the multifilament thread into the analogous monofilament thread overview ($\delta \leq T_c$). (a) Multifilament thread. (b) Equivalent monofilament thread provided with the conductive coating. (c) Equivalent monofilament thread.

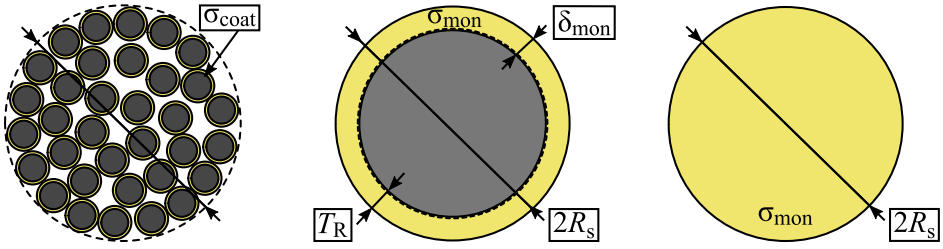

FIGURE 9. Translation from the multifilament thread into the analogous monofilament thread overview ($\delta > T_c$). (a) Multifilament thread. (b) Equivalent monofilament thread provided with the conductive coating. (c) Equivalent monofilament thread.

coating (σ_{coat}).

$$\sigma_{mon} \cdot (2 \cdot R_S \cdot \sqrt{\frac{1}{\pi f \mu \sigma_{mon}}} - \frac{1}{\pi f \mu \sigma_{mon}}) = N_{fil} \cdot \sigma_{coat} \cdot (2 \cdot R_f \cdot \sqrt{\frac{1}{\pi f \sigma_{coat}}} - \frac{1}{\pi f \mu \sigma_{coat}}) \quad (10)$$

Once the σ_{mon} is calculated, the electromagnetically equivalent monofilament threads can be simulated using the same radius, R_S, and the σ_{mon}. The beforementioned translation procedure from the multifilament conductive thread into its equivalent monofilament thread is summarized in Figure 8.

2) THE SKIN DEPTH IS GREATER THAN THE THICKNESS OF THE CONDUCTIVE COATING

Nevertheless, the calculated skin depth in (1) may have been greater than the thickness of the conductive coating applied to each filament, $\delta > T_c$. In this case, the resistance per unit length of the multifilament thread can be calculated using (11), where the parameter δ has been substituted with T_c in comparison to the expression in (5).

$$(R/l) = \frac{1}{N_{fil} \cdot \sigma_{coat} \cdot \pi \cdot (2 \cdot R_f \cdot T_c - T_c^2)} \quad (11)$$

As a result, the value of the electrical conductivity of the equivalent monofilament, σ_{mon}, can be calculated using (12), where σ_{mon} depends on the cross section of the equivalent monofilament (R_S), the frequency (f), the number of filaments which compose each multifilament thread (N_{fil}), the magnetic permeability (μ), the electrical conductivity of the coating (σ_{coat}) and the thickness of the conductive coating applied to each filament (T_c). The already mentioned translation procedure from the multifilament conductive thread into its equivalent monofilament thread is summarized in Figure 9.

$$\sigma_{mon} \cdot (2 \cdot R_S \cdot \sqrt{\frac{1}{\pi f \mu \sigma_{mon}}} - \frac{1}{\pi f \mu \sigma_{mon}}) = N_{fil} \cdot \sigma_{coat} \cdot (2 \cdot R_f \cdot T_c - T_c^2) \quad (12)$$

Comparing the expression in (10) with the expression in (12), there is an important difference. While in (10) the thickness of the conductive coating does not appear in the equation due to the fact that it is sufficiently thick, in (12), this thickness, T_c, is determinant in order to calculate the equivalent electrical conductivity, σ_{mon}. With the aim of summarizing the employed notation in the previous paragraphs, Table 1 presents the parameters and their corresponding meanings.

3) EXAMPLE OF APPLICATION AND VALIDATION

The aforementioned methodology to obtain the equivalent conductive monofilament has been validated in simulations. For this purpose, a multifilament thread has been introduced in a rectangular waveguide, parallel to the orientation of the electric field, $\vec{E}$, and the scattering parameters have been calculated. The simulated thread is composed of $N_{fil} = 19$ filaments, whose radius –including the coating– is $R_f = 31\ \mu$m. The employed thickness of the silver coating of each filament

TABLE 1. Notation employed for the translation from conductive multifilament threads to monofilament threads.

Parameter	Meaning
σ_{coat}	Electrical conductivity of the coating
σ_{mon}	Electrical conductivity of the equivalent monofilament
δ	Calculated skin depth using σ_{coat}
δ_{mon}	Calculated skin depth using σ_{mon}
N_{fil}	Number of filaments which compose the multifilament thread
R_S	Equivalent radius of the multifilament (and monofilament)
R_f	Radius of one filament which composes the multifilament thread
T_c	Thickness of the coating of each filament
T_R	Thickness of the coating of the equivalent monofilament
S_f	Conductive area of the cross section of each filament
S_{mon}	Conductive area of the cross section of the monofilament
$(R/l)_f$	Resistance per unit length of each filament
(R/l)	Resistance per unit length of the complete multifilament thread
$(R/l)_{mon}$	Resistance per unit length of the equivalent monofilament

is $T_c = 0.5\ \mu$m. These filaments compose a multifilament thread whose equivalent radius is $R_S = 0.075$ mm.

The ideal air-filled rectangular waveguide employed in this validation has been simulated using a perfect electric conductor (PEC). The dimensions of the waveguide are its width, height and length, which correspond to $W_{RW} = 20$ mm, $H_{RW} = 10$ mm and $L_{RW} = 25$ mm, respectively. The length of the thread is, also, H_{RW}. Figure 10 depicts the simulation set-up and the corresponding magnifications of the multifilament and monofilament threads.

Applying the methodology described in the previous paragraphs and using $\sigma_{coat} = 6.28 \cdot 10^7$ S/m, which is the electrical conductivity of the silver, the skin depth is $\delta = 0.7328\ \mu$m. The skin depth has been found to be greater than the thickness of the silver coating, consequently the second part of the procedure, summarized in the expression (12), must be employed. As a result, the equivalent conductivity of the monofilament thread has been found to be $\sigma_{mon} = 4.3863 \cdot 10^8$ S/m. Due to the fact that the skin depth is greater than T_c, the multifilament thread must be simulated as a dielectric thread with a silver coating.

Therefore, the scattering parameters have been calculated in the range of frequencies in which the waveguide presents its single-mode operation, $f \in [7.5, 15]$ GHz. Figure 11 depicts the simulated scattering parameters for both cases: using the multifilament thread and using the equivalent monofilament thread with σ_{mon}. A good agreement between both simulations has been obtained, validating the procedure.

C. WOVEN STRUCTURES USING THE MM

1) DESCRIPTION OF THE WOVEN STRUCTURES

Once the multifilament threads have been translated into their equivalent monofilaments, a woven structure can be designed. This woven structure will coincide with the real structure during the fabrication process. As it has been previously explained in Section II, a woven structure is composed of two types of threads, the warp threads and the weft threads, respectively, as generically depicted in Figure 12.

Two different parameters, closely related to the density of the woven structure, can be defined for its accurate characterization. These parameters are the number of ends per inch, *epi*, and the number of picks per inch, *ppi*. The *epi* parameter represents the number of warp ends per inch, as depicted in Figure 13, whereas the *ppi* parameter represents the number of weft threads per inch, as represented in Figure 14.

When working with conductive materials, increasing the values of the *epi* and *ppi* parameters is of interest in order to achieve a dense woven structure. This means that the size of the possible air gaps between the conductive threads can be dramatically reduced. As a result, the currents can flow through the woven structure as if it were a homogeneous conductive material. Additionally, regarding the dielectric materials, modifying the values of the *epi* and *ppi* parameters is completely related to the resultant equivalent relative permittivity, ϵ_{eq}.

In order to design a woven structure using the MM, several factors have to be taken into account. First, depending on the dimensions of the cross section and rigidity of the different employed materials, a woven structure can adopt one of the following two approaches. Either the warp threads are more rigid and the weft threads tend to conform the woven structure around the warp threads, while the warp threads remain straight, as depicted in Figure 12a, or vice versa as occurs in Figure 12b. Secondly, the *epi* and *ppi* parameters, which will depend on the characteristics of the industrial loom and the procedure employed to manufacture the woven structure, must be known. Figure 15 summarizes the procedure to design a woven structure.

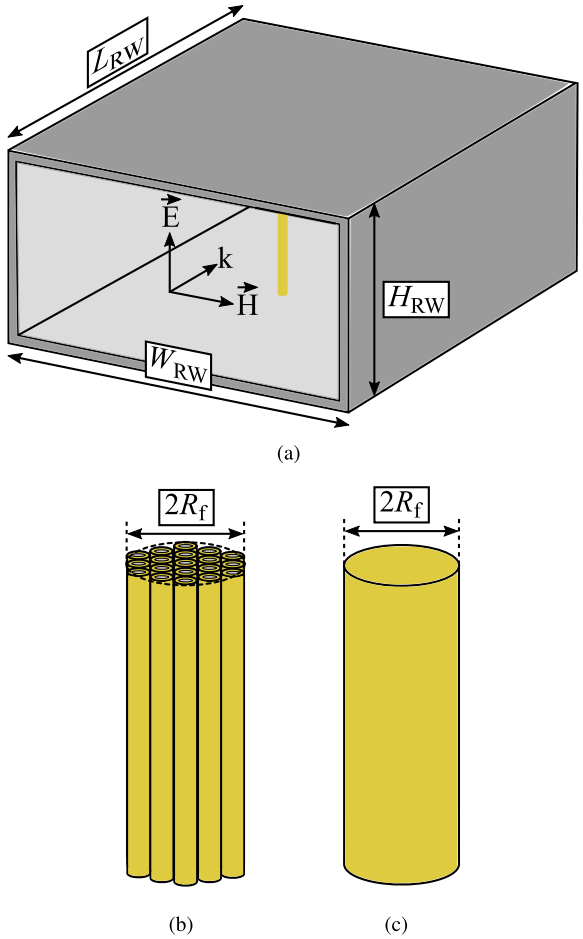

FIGURE 10. Simulated set-up for the translation between conductive multifilament and monofilament threads. (a) Set-up overview. (b) Magnification of the multifilament thread. (c) Magnification of the monofilament thread.

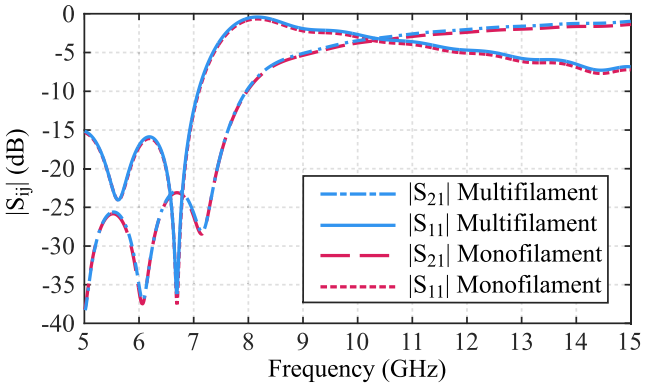

FIGURE 11. Comparison of the simulated scattering parameters of the equivalence between conductive multifilament and monofilament threads.

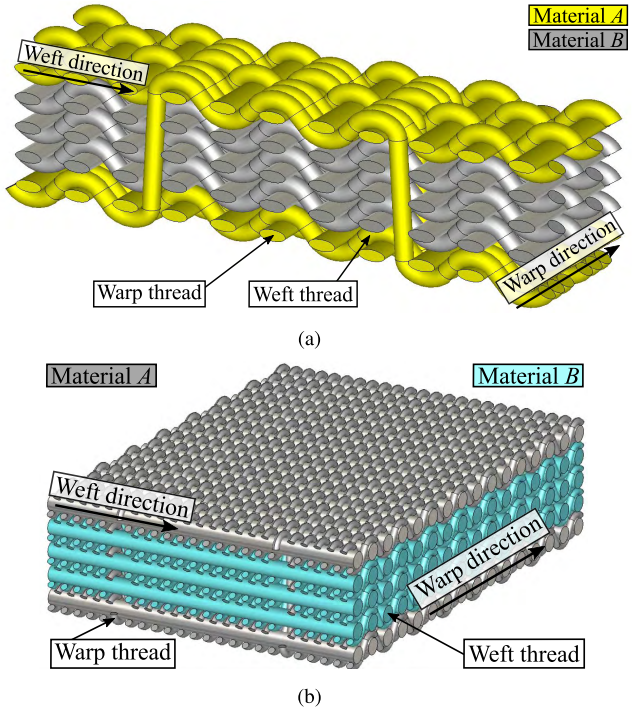

FIGURE 12. Generic multilayered woven structures using the MM and different materials. (a) Rigid warp threads. (b) Rigid weft threads.

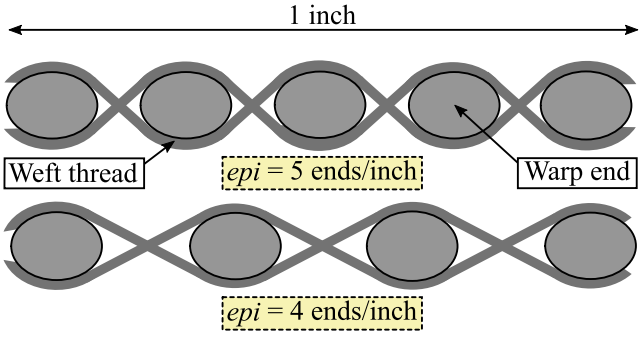

FIGURE 13. Schematic representation of the *epi* parameter (front view of the woven structure).

2) MATHEMATICAL PARAMETRIC CHARACTERISATION

Although different approaches to characterize the deformed cross section of the threads can be used, as explained in section IV, the most employed one is the Pierce's elliptic cross section. For this reason, the herein presented parameterization of a woven structure will be described assuming that all the cross sections have been modeled with the Pierce's elliptic approximation, therefore, as ellipses. Consequently, a mathematical modeling of the paths of the non-rigid threads in the structure is required. For this purpose, these paths have been mathematically modeled as ellipse arcs and tangent lines.

Assuming that the threads which remain straight are the warp threads, and the weft threads conform the woven structure, finding the tangent points given a pair of ellipses is required. Given two generic ellipses, denoted by E_0 and E_1, as depicted in Figure 16, they represent the cross sections of two consecutive warp ends. Nevertheless, an analogous modeling can be employed if the threads which remain straight are the weft threads.

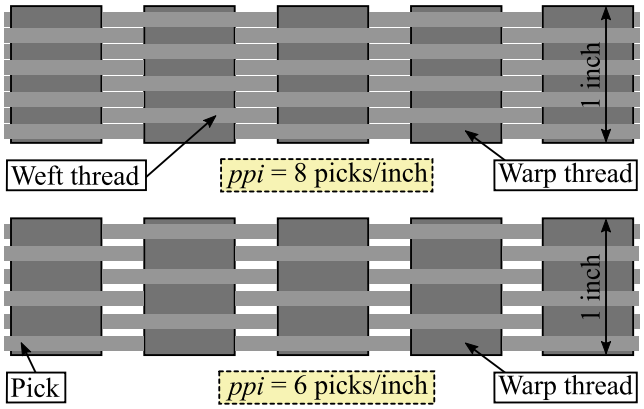

FIGURE 14. Schematic representation of the *ppi* parameter (side view of the woven structure).

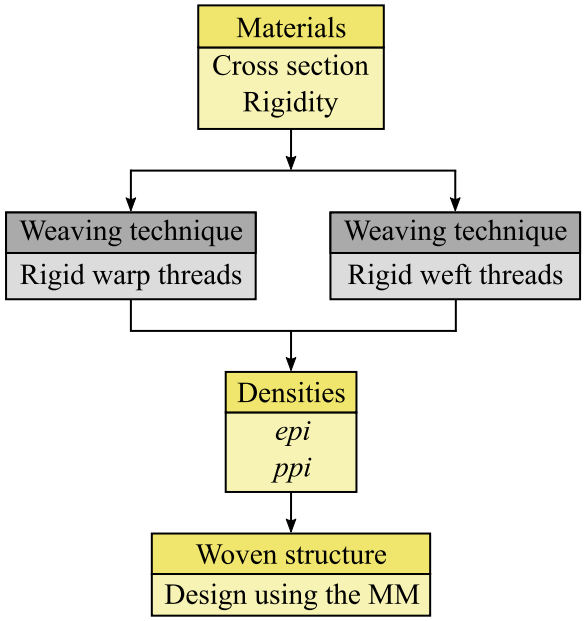

FIGURE 15. Block diagram to summarise the procedure of designing a woven structure.

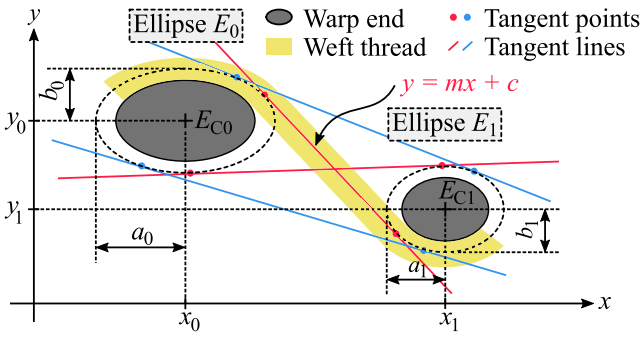

FIGURE 16. Generic mathematical modeling based on ellipses and tangents.

As these warp threads may belong to different layers of the multilayered woven structure or be composed of different materials, the corresponding ellipses are defined by the coordinates of their centers, $E_{C0} = (x_0, y_0)$ and $E_{C1} = (x_1, y_1)$, and the dimensions of their semiaxes, $\{a_0, b_0\}$ and $\{a_1, b_1\}$, respectively, and consequently a generic mathematical modeling is presented. The parametric equations to define either ellipse, with $\theta \in [0, 2\pi)$, are given by (13b) and (13).

$$E_{x0} = a_0 cos(\theta) + x_0 \tag{13a}$$
$$E_{y0} = b_0 sin(\theta) + y_0 \tag{13b}$$
$$E_{x1} = a_1 cos(\theta) + x_1 \tag{14a}$$
$$E_{y1} = b_1 sin(\theta) + y_1 \tag{14b}$$

If a solution exists, then, four different lines are tangent to both ellipses. A line can be defined by two parameters, its slope, m, and its y-axis intercept, c. Thus, the generic line is defined by $y = mx + c$. By setting the equation of the line equal to (13b) and (13), or to their equivalent cartesian mathematical expressions, and imposing on the line the condition of being tangent to both ellipses, only a point of each ellipse must coincide with a point of the line. For this purpose, the discriminant functions of the resultant expressions must be equal to zero. Therefore, the second order system of equations in (15) is generated.

$$\begin{cases} -2b_0^2x_0 - 2ma_0^2(y_0 - c)^2 + (-4(b_0^2 + a_0^2m^2) \\ \quad (x_0^2b_0^2 + a_0^2(y_0 - c)^2 - a_0^2b_0^2) = 0 \\ -2b_1^2x_1 - 2ma_1^2(y_1 - c)^2 + (-4(b_1^2 + a_1^2m^2) \\ \quad (x_1^2b_1^2 + a_1^2(y_1 - c)^2 - a_1^2b_1^2) = 0 \end{cases} \tag{15}$$

The solution of (15) returns the slopes and the intercepts of the four different lines that are tangent to the ellipses, which are denoted by m_i and c_i, with $i \in [1, 4]$. From the slopes and the intercepts, the tangent points (x_{p0_i}, y_{p0_i}) and (x_{p1_i}, y_{p1_i}), for E_0 and E_1 respectively, can be worked out as shown in (16) and (17).

$$x_{p0\_i} = -\frac{-2b_0^2x_0 - 2m_ia_0^2(y_0 - c_i)}{2(b_0^2 + a_0^2m_i^2)} \tag{16a}$$
$$y_{p0\_i} = m_ix_{p0\_i} + c_i \tag{16b}$$
$$x_{p1\_i} = -\frac{-2b_1^2x_1 - 2m_ia_1^2(y_1 - c_i)}{2(b_1^2 + a_1^2m_i^2)} \tag{17a}$$
$$y_{p1\_i} = m_ix_{p1\_i} + c_i \tag{17b}$$

Once the tangent points have been worked out, the paths of the weft threads are defined and the woven structure is completely characterized. Figure 17 depicts different views of a generic multilayered woven structure, where an example of the ellipses, the tangent points and the tangent line is indicated.

The MM is very useful in order to design the woven structure for the potential prototypes based on smart textile (antennas, tags or frequency selective surfaces, among others). For this reason, several commercial software packages can be found in order to represent the MM, although neither of them can electromagnetically simulate the structure.

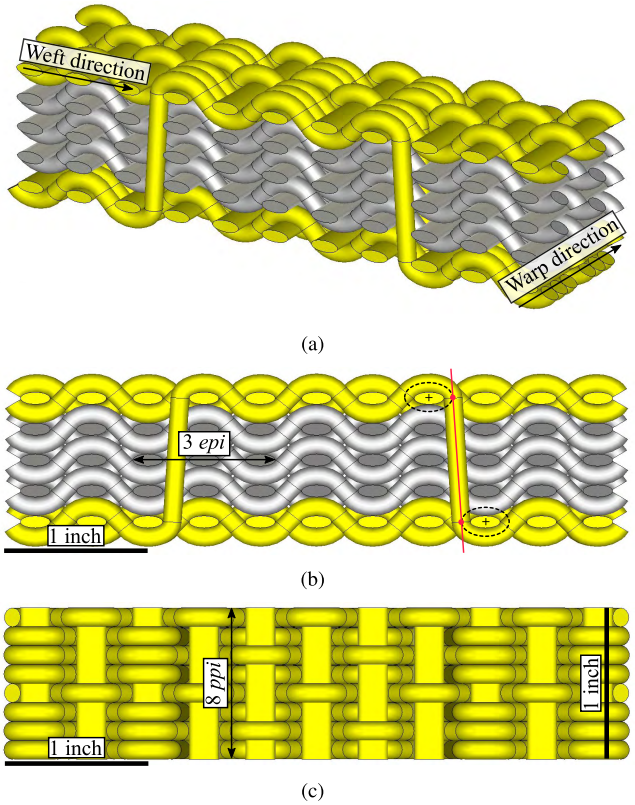

FIGURE 17. Generic multilayered woven structure using rigid warp threads and two materials, conductive (yellow) and dielectric (grey). (a) Woven structure overview. (b) Front view and *epi* parameter. (c) Top view and *ppi* parameter.

Some of these software packages are TexGen [41], which has been implemented in order to simulate textile composites, or 3DWeave [42], which has been thought to be of help for textile design. The MM design can be imported in modern electronic industrial jacquard looms.

Moreover, despite the fact that the representations of the MM with the beforementioned software packages can be imported in, for example, STL (stereolithography) format and used in commercial electromagnetic simulators such as High Frequency Structure Simulator (HFSS) [43] or Computer Simulation Technology (CST) Microwave Studio [44], the parameterization of the structure is completely lost during this process. For this reason, in this paper, a complete parameterization of the woven structure is proposed to be used directly in commercial electromagnetic simulators such as HFSS or CST.

V. LAYERS MODEL

As it has been mentioned before, a woven structure designed using the MM is directly translatable into a manufactured prototype. Nevertheless, finding a computationally simpler modeling is required in order to simulate larger and more complex structures. For this reason, the LM is proposed.

The LM is defined using an homogeneous dielectric substrate whose relative permittivity and loss tangent are denoted by ϵ_{eq} and $\tan(\delta)_{eq}$, respectively, and an electrical conductivity denoted by σ_{eq}. Depending on the electromagnetic behavior of the threads, electrically conductive or dielectric, a different procedure to translate from the MM to the LM is employed.

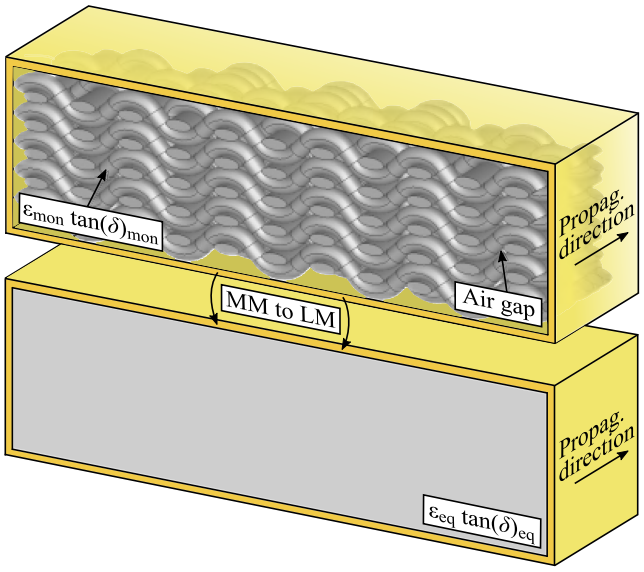

FIGURE 18. Translation from the MM into the LM outline applied to dielectric monofilaments using the waveguide based methodology.

A. DIELECTRIC MATERIALS

Due to the air gaps between the dielectric monofilaments which conform the woven structure, the relative permittivity of the equivalent dielectric substrate is reduced and denoted by ϵ_{eq}. Additionally, a new loss tangent can be defined and denoted by $\tan(\delta)_{eq}$.

To translate the MM into the LM, a theoretical method has been used. For this purpose, the ϵ_{mon} and $\tan(\delta)_{mon}$, as well as the *epi* and *ppi* parameters must be taken into account. Simulating a rectangular waveguide which has been filled with monofilaments (ϵ_{mon} and $\tan(\delta)_{mon}$), using the same *epi* and *ppi* densities as the dielectric substrate has in the woven structure, and comparing its electromagnetic behavior with another rectangular waveguide which has been homogeneously filled, the corresponding ϵ_{eq} and $\tan(\delta)_{eq}$ parameters can be easily extracted from the cut-off frequency and the insertion losses as summarized in Figure 18. Therefore, the dielectric parameters of the MM can be translated into their corresponding of the LM. As a result, the LM corresponds to the conventional procedure employed to simulate microwave antennas or circuits based on rigid substrates.

Consequently, the relative dielectric permittivity is first reduced from the FM to the MM due to the air gaps between the filaments which conform the thread, transforming ϵ_{fil} into ϵ_{mon}. Analogously, the relative dielectric permittivity is then reduced again from the MM to the LM due to the air gaps between the monofilaments which conform the equivalent woven structure, transforming ϵ_{mon} into ϵ_{eq}.

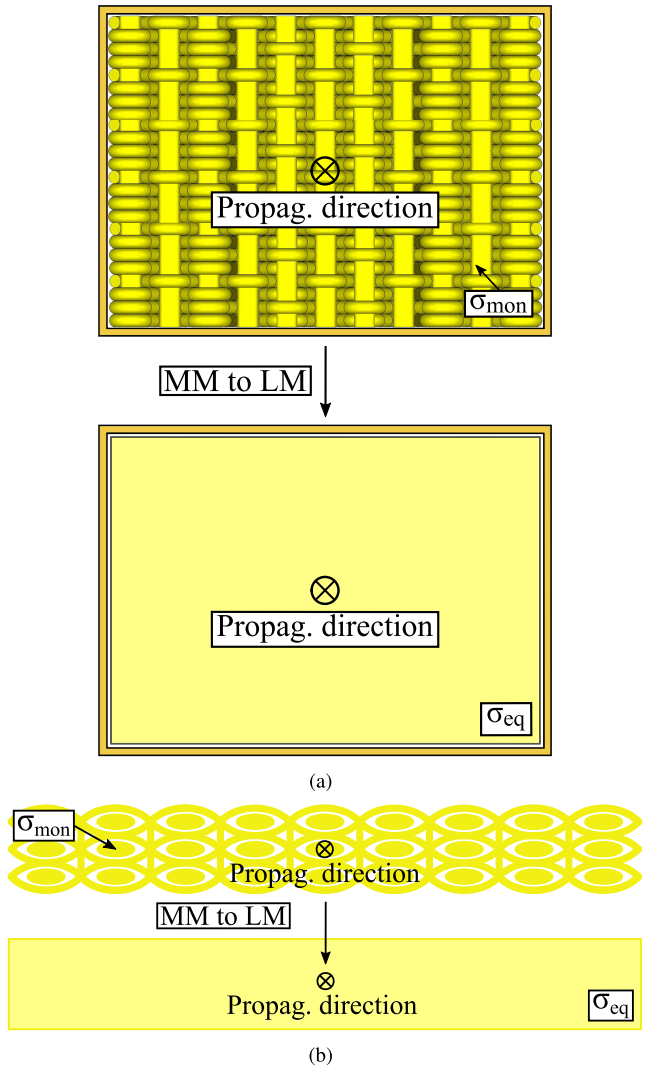

FIGURE 19. Translation from the MM into the LM outline applied to conductive monofilaments using a rectangular waveguide. (a) Woven structure perpendicular to the propagation direction. (b) Woven structure parallel to the propagation direction.

B. CONDUCTIVE MATERIALS

To translate the conductive monofilaments, described by σ_{mon}, from the MM into a homogeneous conductive material, characterized by σ_{eq}, for the LM, two different situations can be analyzed. When the behavior of the woven structure needs to be studied when it is perpendicular to the propagation direction, a square-shaped woven MM structure can be simulated inside a rectangular waveguide, perpendicular to its propagation direction. Its electromagnetic behavior, in terms of the scattering parameters is then compared to a homogeneous conductive square-shaped sheet, using the same dimensions and a conductivity given by σ_{eq} as summarized in Figure 19a. This can be used for the design of woven FSS or planar absorbers.

Alternatively, when the behavior of the MM of the woven structure, described by σ_{mon}, needs to be analyzed when it is parallel to the propagation direction, the multilayered fabric can be put inside a rectangular waveguide, parallel to the propagation direction, as depicted in Figure 19b. Its electromagnetic behavior can then be compared to a homogeneous conductive rectangular-shaped sheet, with the same dimensions and a conductivity given by σ_{eq}. This procedure can be employed for the development of TIW (textile integrated waveguide) or microstrip woven antennas.

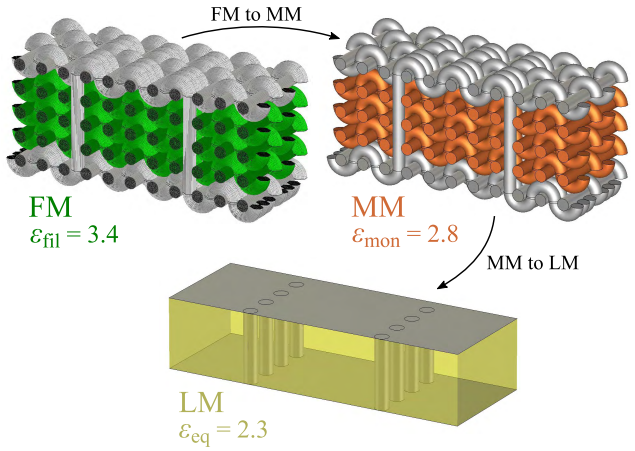

FIGURE 20. Different FM, MM and LM of the structure of a TIW example.

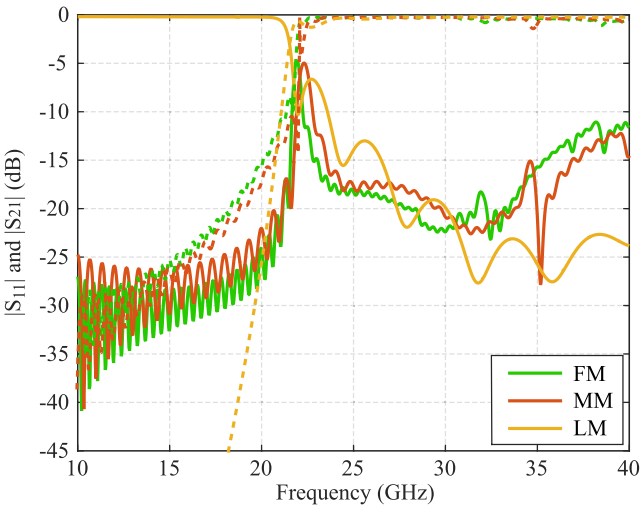

FIGURE 21. Equivalence between FM, MM and LM for a TIW example.

C. EQUIVALENCE BETWEEN FM, MM AND LM

In order to demonstrate the validity of the equivalence between the three different models previously explained, in the section, an example using the textile translation of a SIW (substrate integrated waveguide) is presented. In this case, for simplification, PEC has been employed as conductive material, so that the objective is the validation of the three-step modeling regarding the dielectric materials. For this purpose, the three different structures represented in Figure 20 have been employed, being the cut-off frequency, f_c, of the waveguides 22 GHz.

As a result, the different relative permittivities are $\epsilon_{fil} = 3.4$, $\epsilon_{mon} = 2.8$ and $\epsilon_{eq} = 2.3$, respectively. Consequently, in Figure 21 the scattering parameters corresponding to the

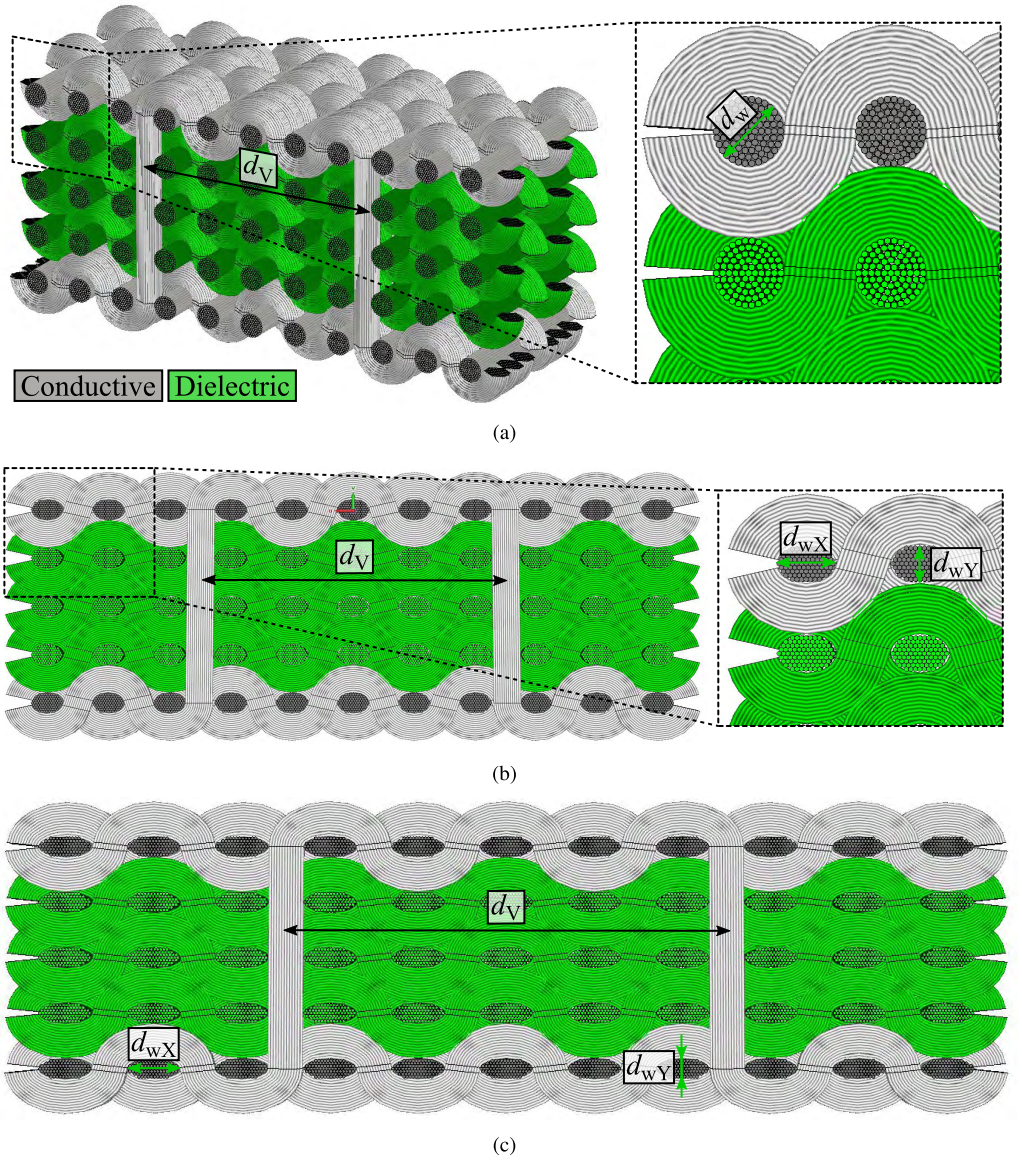

FIGURE 22. Deformation of the woven structures overview. (a) Initial circular cross section overview and corresponding magnification. (b) Elliptic cross section (smaller eccentricity) and corresponding magnification. (c) Elliptic cross section (bigger eccentricity).

different models are represented. It is important to take into account that, due to having employed different solvers to calculate the scattering parameters for the models, the values below the cut-off frequency can differ. As a consequence, the LM has been calculated using a frequency domain solver and the value of the $|S_{11}|$ is near zero. Nevertheless, a time domain solver has to be employed to simulate both the FM and the MM due to the complex mesh and the value of the $|S_{11}|$ below the cut-off frequency is not coherent, although is a well known issue using the commercial software used.

D. DEFORMATION OF WOVEN STRUCTURES

As it has been previously explained, the woven structure depends not only on the employed materials, but also on the *epi* and *ppi* parameters and the forces actuating between the threads. For this reason, the same materials may present different cross sections depending on the woven structure in which they are employed. As a consequence, the translation between the different models may lead to different results.

Figure 22 depicts an overview of the deformation of the woven structures. Figure 22a represents a hypothetical translation of a SIW into a completely woven structure or, simply, a TIW, using rigid warp threads. A SIW is composed of a dielectric substrate between two metallic plates. The plates are connected using two rows of conductive vias [45]. A SIW has been first translated into a TIW in [34]. For this purpose, the substrate has been composed of warp and weft dielectric threads, whereas the conductive plates have been achieved using conductive yarns. In order to emulate the conductive vias, several conductive very flexible weft threads have been

interwoven during the manufacturing process connecting the different layers which compose the multilayered woven structure.

In this paper, the example presented in Figure 22, in which the dielectric and conductive materials are green and grey colored, respectively, and the electromagnetic field propagates in the direction parallel to the rigid warp threads, has been proposed with the aim of clarifying the deformation of the woven structures and the corresponding effect in the three-step modeling.

Figure 22a represents a woven structure whose threads are provided with circular cross sections, consequently with circumferences whose diameter is denoted d_{W}. These threads are composed of N_{fil} filaments whose diameters are denoted by d_{fil}. Besides, the distance between the centers of the conductive vias of the woven SIW, which is inversely related to the cut-off frequency of the SIW, is denoted by d_{V}.

Analogously, Figure 22b depicts a similar structure. Nevertheless, the cross sections of the threads have been modified due to the reorganization of the filaments inside the thread, and now they conform elliptic cross sections, whose horizontal and vertical axes are d_{wX} and d_{wY}, respectively. Figure 22c also depicts a similar structure, although the ellipses present a bigger eccentricity compared to the ellipses in Figure 22b, due to the new distribution of the filaments in the thread. The phenomenon which studies the deformation of these ellipses is known as buckling [46].

The different buckling effects experimented by the circumference and the ellipses in the representations of Figure 22 lead to two consequences. First, the bigger the eccentricity of the ellipses, the bigger the distance between the conductive vias, due to the separation between the warp threads. Second, the modification of the eccentricity of the ellipses and the corresponding variation of the distance d_{V}, lead to the modification of the distribution of the air gaps between the threads.

As a result, the equivalent relative permittivity of the woven structure inside the TIW is modified, even though the materials remain being the same. For example, if the following relation is made between these parameters: $d_{\mathrm{wY}} = d_{\mathrm{W}} - 4 \cdot n \cdot d_{\mathrm{fil}}$, being d_{wX} the corresponding so that the perimeter of the cross section remains constant, and n a variable to control the eccentricity (known as the deformation index), a relation between the cut-off frequency of the structure and n, as well as between the equivalent relative permittivity ϵ_{eq} of the structure and n can be worked out.

Figure 23 depicts the dependence between the equivalent permittivity of the woven structure and the deformation index. The green coloured filaments have been simulated using a relative permittivity of $\epsilon_{\mathrm{fil}} = 3.5$, while the conductive elements –for simplification– have been simulated using perfect electric conductors. As a result, the relation between the cut-off frequency of the woven SIW and n is also represented. As previously mentioned, the bigger the eccentricity of the ellipses, the bigger the distance between the conductive vias. This is due to the increase of the distance between the centers of two consecutive warp threads, *sepx*.

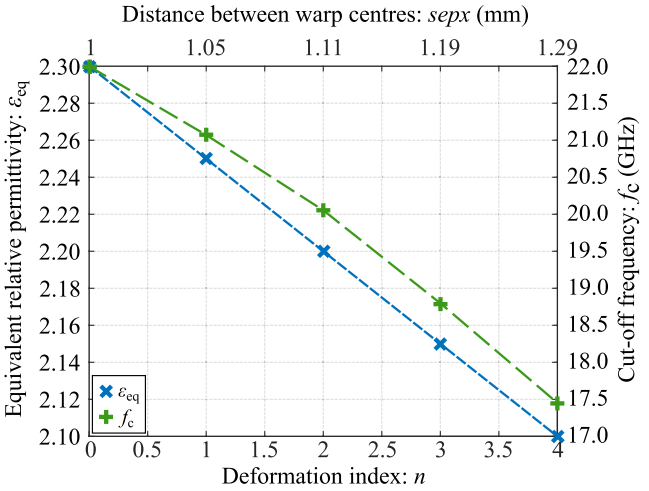

FIGURE 23. Modification of the ϵ_{eq} and the f_{c} of a woven SIW depending on *n* and *sepx*.

VI. VALIDATION: EXAMPLES OF USE

The theory already presented in the previous sections has been put into practice in different works developed by the authors. Partial results have already been presented in these works [34]–[38], not only verifying the theory underneath, but also justifying the necessity of the development and the analysis of these complex woven structures. The most representative results are summarized in the following subsections.

A. MILLIMETRE-WAVE TIW

A millimeter-wave TIW has been developed operating between 32 and 37 GHz, as the first approach of the development of completely textile integrated circuits [34]. It consists of three layers of rigid warp threads, being the middle layer the non-conductive one. Besides, thanks to the weft threads, the different woven patterns are achieved. In Figure 24, both the conventional SIW and the woven TIW are represented in order to clarify the translation into a woven prototype, using the different approximations –circular, elliptic and Kemp's racetrack cross sections– and mathematical expressions already explained in the previous sections to emulate the multifilament threads.

Different prototypes have been manufactured using different lengths (30, 40 and 55 mm, respectively) and their scattering parameters have been measured and compared with the simulations as presented in the bottom part of Figure 24. Nevertheless, the simulations of the conductive materials in [34] have been carried out using a simplified version of the modeling with respect to the one presented in this work. Due to the high value of the losses of these prototypes, in [35], a microwave TIW is presented achieving better results.

B. MICROSTRIP-FED SLOT ANTENNA

A microstrip-fed antenna for dedicated short-range communications (DSRC) has been developed operating at 5.9 GHz

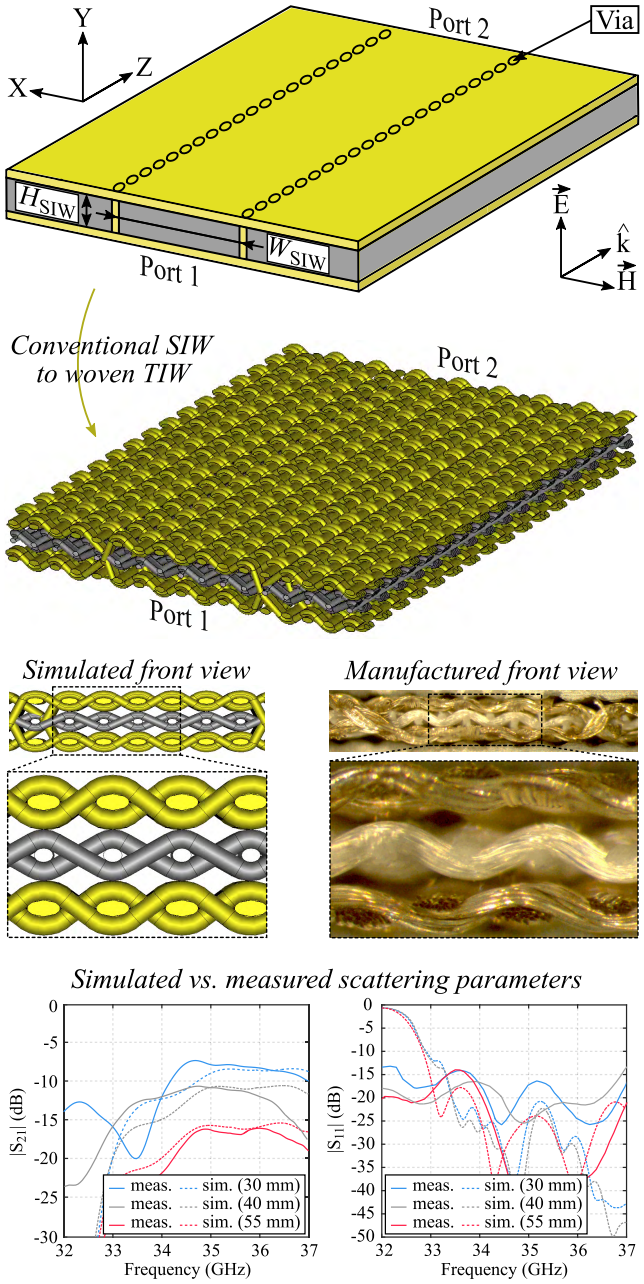

FIGURE 24. Overview of the development of the millimeter-wave TIW example [34].

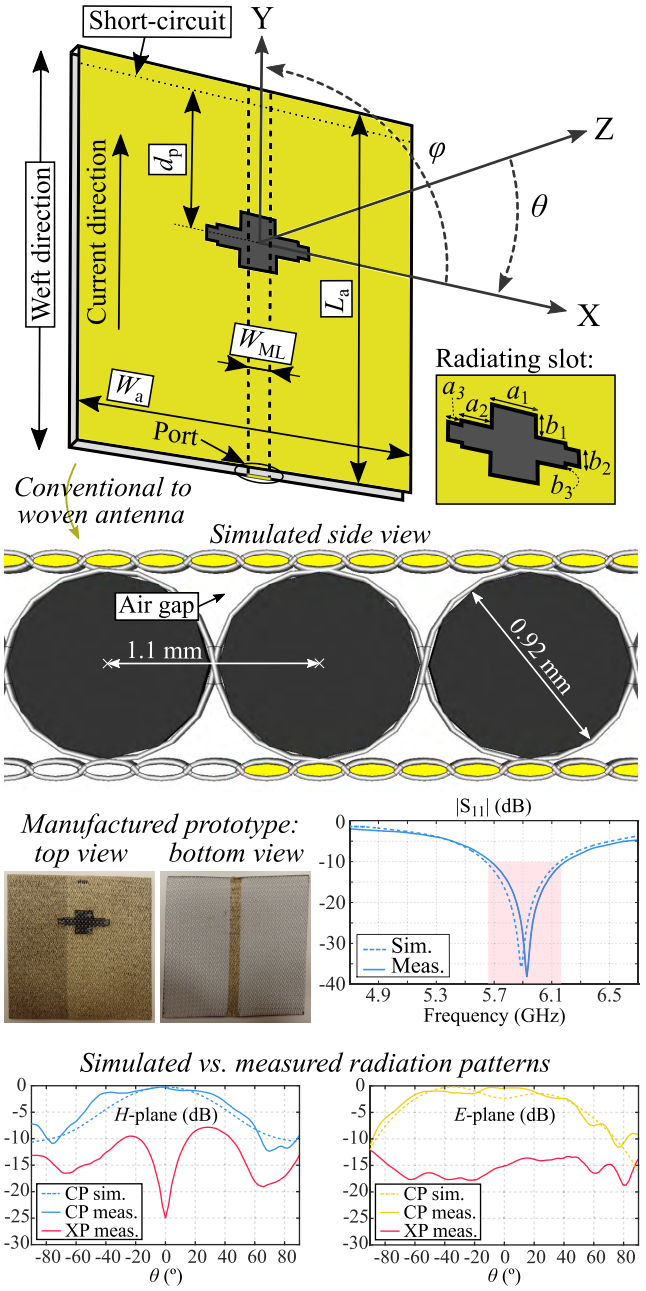

FIGURE 25. Overview of the development of the microstrip-fed slot antenna example [36].

presenting a 9.3% bandwidth [36]. The woven antenna consists of three layers, a conductive ground plane where the radiating slot has been placed, a dielectric substrate and the microstrip line, respectively. The antenna has been manufactured using rigid very thick threads in order to obtain the specific thickness to implement the design, as presented in the sketches in Figure 25.

A prototype has been manufactured. This process consists of weaving the complex woven structure and, then, cutting the radiating slot with a prototyping laser machine, although the slot can be achieved using *ad hoc* industrial looms provided ith a cutting mechanism. Posteriorly, the prototype has been characterized using a PNA-X vector network analyzer to measure the $|S_{11}|$ parameter, and a set-up in the anechoic chamber in order to measure radiation patterns for both the *E*– and the *H*–planes. The measurements have been compared with the simulations, as represented in the bottom part of Figure 25, in order to demonstrate their agreement.

VII. CONCLUSIONS

A three-step modeling has been explained to electromagnetically simulate woven structures. First, a FM has been defined to characterize the different threads, dielectric or conductive, employed in the woven structure. For both, the dielectric

and conductive materials, the deformed cross section of the threads and the number of filaments which form each thread have been taken into account.

Then, a reduction of the computational complexity of the problem is achieved by defining the MM, which substitutes the multifilament threads by electromagnetically equivalent monofilament threads. To translate the FM into the MM for the dielectric threads, the FM and the electromagnetic characteristics of the materials from which the filaments have been extruded are taken into account. In addition, in order to rigorously translate the FM into the MM, the skin depth effect has been taken into account for the conductive materials.

A new model, the LM, has been defined in order to obtain a homogeneous relative permittivity and electrical conductivity, reducing the complexity of the woven structure to a conventional substrate integrated structure. In order to translate the MM into the LM, a parametric characterization of the woven patterns has been analyzed in order to obtain the mathematical equations corresponding to the warp or weft ends, and the corresponding tangent points to define the curves of the flexible threads.

Using the already explained three-step modeling, a designed woven structure can be electromagnetically characterized before its fabrication. Therefore, fully textile integrated circuits and antennas can be easily designed and simulated using the LM, which is equivalent to the conventional method to simulate standard circuits and antennas. Moreover, the LM reduces the computational complexity of the original electromagnetic problem and, therefore, reduces the simulation times, avoiding the simulation of the complete MM of the circuit or antenna.

In order to validate the modeling technique and the electromagnetic analysis, Section VI has been devoted to summarize their practical use in the development of different textile integrated circuits such as a TIW and a microstrip-fed antenna. Although in this work a complete and enhanced version of the parametric characterization and electromagnetic analysis is presented, the examples have been developed using simplified versions. Nevertheless, the usefulness of the work is demonstrated with the agreement between simulations and measurements.

REFERENCES

[1] M. Sanchez-Fernandez, A. Tulino, E. Rajo-Iglesias, J. Llorca, and A. G. Armada, "Blended antenna wearables for an unconstrained mobile experience," *IEEE Commun. Mag.*, vol. 55, no. 4, pp. 160–168, Apr. 2017.
[2] D. Blanco and E. Rajo-Iglesias, "Wearable Fabry–Pérot antenna," *IEEE Antennas Wireless Propag. Lett.*, vol. 17, no. 1, pp. 106–109, Jan. 2018.
[3] A. Rida, L. Yang, R. Vyas, S. Bhattacharya, and M. M. Tentzeris, "Design and integration of inkjet-printed paper-based UHF components for RFID and ubiquitous sensing applications," presented at the Eur. Microw. Conf., Munich, Germany, Oct. 2007.
[4] A. Rida, L. Yang, R. Vyas, and M. M. Tentzeris, "Conductive inkjet-printed antennas on flexible low-cost paper-based substrates for RFID and WSN applications," *IEEE Antennas Propag. Mag.*, vol. 51, no. 3, pp. 13–23, Jun. 2009.
[5] V. Lakafosis, A. Rida, R. Vyas, L. Yang, S. Nikolaou, and M. M. Tentzeris, "Progress towards the first wireless sensor networks consisting of inkjet-printed, paper-based RFID-enabled sensor tags," *Proc. IEEE*, vol. 98, no. 9, pp. 1601–1609, Sep. 2010.
[6] K. Kirschenmann, K. W. Whites, and S. M. Woessner, "Inkjet printed microwave frequency multilayer antennas," presented at the IEEE Antennas Propag. Soc. Int. Symp., Honolulu, HI, USA, Jun. 2007.
[7] J. Virtanen *et al.*, "The effect of conductor thickness in passive inkjet printed RFID tags," presented at the IEEE Antennas Propag. Soc. Int. Symp., Toronto, ON, Canada, Jul. 2010.
[8] A. Kanso *et al.*, "Inkjet printing of coplanar wire-patch antenna on a flexible substrate," presented at the Int. Symp. Antenna Technol. Appl. Electromagn., Toulouse, France, Jun. 2012.
[9] A. A. Babar *et al.*, "Inkjet-printable UHF RFID tag antenna on a flexible ceramic- polymer composite substrate," presented at the IEEE/MTT-S Int. Microw. Symp. Dig., Montreal, QC, Canada, Jun. 2012.
[10] A. Chauraya *et al.*, "Inkjet printed dipole antennas on textiles for wearable communications," *IET Microw., Antennas Propag.*, vol. 7, no. 9, pp. 760–767, Jun. 2013.
[11] W. G. Whittow, Y. Li, R. Torah, K. Yang, S. Beeby, and J. Tudor, "Printed frequency selective surfaces on textiles," *Electron. Lett.*, vol. 50, no. 13, pp. 916–917, 2014.
[12] W. G. Whittow *et al.*, "Inkjet-printed microstrip patch antennas realized on textile for wearable applications" *IEEE Antennas Wireless Propag. Lett.*, vol. 13, pp. 71–74, 2014.
[13] G. Ginestet *et al.*, "Embroidered antenna-microchip interconnections and contour antennas in passive UHF RFID textile tags," *IEEE Antennas Wireless Propag. Lett.*, vol. 16, pp. 1205–1208, Nov. 2017.
[14] A. Paraskevopoulos, D. de Sousa Fonseca, R. D. Seager, W. G. Whittow, J. C. Vardaxoglou, and A. A. Alexandridis, "Higher-mode textile patch antenna with embroidered vias for on-body communication," *IET Microw., Antennas Propag.*, vol. 10, no. 7, pp. 802–807, May 2016.
[15] B. Ivsic, D. Bonefacic, and J. Bartolic, "Considerations on embroidered textile antennas for wearable applications," *IEEE Antennas Wireless Propag. Lett.*, vol. 12, pp. 1708–1711, Dec. 2013.
[16] S. Zhang, A. Paraskevopoulos, C. Luxey, J. Pinto, and W. Whittow, "Broad-band embroidered spiral antenna for off-body communications," *IET Microw., Antennas Propag.*, vol. 10, no. 13, pp. 1395–1401, 2016.
[17] T. Acti *et al.*, "Embroidered wire dipole antennas using novel copper yarns," *IEEE Antennas Wireless Propag. Lett.*, vol. 14, pp. 638–641, 2015.
[18] Z. Wang, L. Z. Lee, D. Psychoudakis, and J. L. Volakis, "Embroidered multiband body-worn antenna for GSM/PCS/WLAN communications," *IEEE Trans. Antennas Propag.*, vol. 62, no. 6, pp. 3321–3329, Jun. 2014.
[19] M. M. Tahseen and A. A. Kishk, "Flexible and portable textile-reflectarray backed by frequency selective surface," *IEEE Antennas Wireless Propag. Lett.*, vol. 17, no. 1, pp. 46–49, Jan. 2018.
[20] R. R. G. Perron, G. C. Huang, and M. F. Iskander, "Textile electromagnetic coupler for monitoring vital signs and changes in lung water content," *IEEE Antennas Wireless Propag. Lett.*, vol. 14, pp. 151–154, 2015.
[21] D. Ferreira, P. Pires, R. Rodrigues, and R. F. S. Caldeirinha, "Wearable textile antennas: Examining the effect of bending on their performance," *IEEE Antennas Propag. Mag.*, vol. 59, no. 3, pp. 54–59, Jun. 2017.
[22] R. Moro, S. Agneessens, H. Rogier, A. Dierck, and M. Bozzi, "Textile microwave components in substrate integrated waveguide technology," *IEEE Trans. Microw. Theory Techn.*, vol. 63, no. 2, pp. 422–432, Feb. 2015.
[23] P. J. Soh, G. A. E. Vandenbosch, S. L. Ooi, and N. H. M. Rais, "Design of a broadband all-textile slotted PIFA," *IEEE Trans. Antennas Propag.*, vol. 60, no. 1, pp. 379–384, Jan. 2012.
[24] T. Haagenson, S. Noghanian, P. de Leon, and Y.-H. Chang, "Textile antennas for spacesuit applications: Design, simulation, manufacturing, and testing of textile patch antennas for spacesuit applications," *IEEE Antennas Propag. Mag.*, vol. 57, no. 4, pp. 64–73, Aug. 2015.
[25] S. Zhu and R. Langley, "Dual-band wearable textile antenna on an EBG substrate," *IEEE Trans. Antennas Propag.*, vol. 57, no. 4, pp. 926–935, Apr. 2009.
[26] J. Lilja, P. Salonen, T. Kaija, and P. D. Maagt, "Design and manufacturing of robust textile antennas for harsh environments," *IEEE Trans. Antennas Propag.*, vol. 60, no. 9, pp. 4130–4140, Sep. 2012.
[27] T. C. Baum, R. W. Ziolkowski, K. Ghorbani, and K. J. Nicholson, "Investigations of a load-bearing composite electrically small Egyptian axe dipole antenna," *IEEE Trans. Antennas Propag.*, vol. 65, no. 8, pp. 3827–3837, Aug. 2017.
[28] Y. Senbokuya and H. Tsunoda, "A study on the circular patch antennas using conductive non-woven fiber fabrics," presented at the IEEE Antennas Propag. Soc. Int. Symp., San Antonio, TX, USA, Jun. 2002.
[29] Y. Jiang *et al.*, "A highly usable and customizable sEMG sensor for prosthetic limb control using polypyrrole-coated nonwoven fabric sheet," presented at the IEEE SENSORS, Busan, South Korea, Nov. 2015.

[30] R. Polansky *et al.*, "A study on the usage of nonwoven nanofibers in electrical insulating materials," presented at the IEEE Conf. Electr. Insul. Dielectr. Phenomena, Ann Arbor, MI, USA, Oct. 2015.
[31] A. N. Austin, J. F. Dawson, I. D. Flintoft, and A. C. Marvin, "Analysis of the shielding properties of metalised nonwoven materials," presented at the Int. Symp. Electromagn. Compat., Brugge, Belgium, Sep. 2013.
[32] S. Gangopadhyay *et al.*, "Design and development of electro-conductive rectangular textile antenna using polypropylene fabric," presented at the IEEE Uttar Pradesh Sect. Int. Conf. Electr., Comput. Electron., Mathura, India, Jan. 2017.
[33] T. M. Nguyen and J.-Y. Chung, "Parametric study on radiation efficiency of woven textile antennas," presented at the Int. Workshop Antenna Technol. (iWAT), Seoul, South Korea, 2015, pp. 117–119.
[34] L. Alonso-González, S. Ver-Hoeye, C. Vázquez-Antuña, M. Fernández-García, and F. L.-H. Andrés, "On the techniques to develop millimeter-wave textile integrated waveguides using rigid warp threads," *IEEE Trans. Microw. Theory Techn.*, vol. 66, no. 2, pp. 751–761, Feb. 2018.
[35] L. Alonso-González, S. Ver-Hoeye, M. Fernández-García, and F. L.-H. Andrés, "Three-dimensional fully interlaced woven microstrip-fed substrate integrated waveguide," *Prog. Electromagn. Res.*, vol. 163, pp. 25–38, 2018. [Online]. Available: http://www.jpier.org/PIER/pier.php?paper=18040207
[36] L. Alonso-González *et al.*, "Fully textile-integrated microstrip-fed slot antenna for dedicated short-range communications," *IEEE Trans. Antennas Propag.*, vol. 66, no. 5, pp. 2262–2270, May 2018.
[37] L. Alonso-González, S. Ver-Hoeye, M. Fernández-García, and F. L.-H. Andrés, "Layer-to-layer angle interlock 3D woven bandstop frequency selective surface," *Prog. Electromagn. Res.*, vol. 162, pp. 81–94, 2018.
[38] L. Alonso-González, S. Ver-Hoeye, M. Fernández-García, and F. L.-H. Andrés, "Broadband flexible fully textile-integrated bandstop frequency selective surface," *IEEE Trans. Antennas Propag.*, vol. 66, no. 10, pp. 5291–5299, Oct. 2018.
[39] J. Hu, *Structure and Mechanics of Woven Fabrics*. New York, NY, USA: Woodhead Publishing, 2004, pp. 63–66.
[40] K. Rabaani and N. Boulejfen, "Characteristic impedance and propagation constant assessment of substrate integrated waveguide transmission line," presented at the 11th Int. Design Test Symp. (IDT), Hammamet, Tunisia, Dec. 2016.
[41] H. Lin, L. P. Brown, and A. C. Long, "Modelling and simulating textile structures using TexGen," *Adv. Mater. Res.*, vol. 331, pp. 44–47, Sep. 2011.
[42] The DesignScope Company. *3DWeave*. Accessed: Nov. 20, 2018. [Online]. Available: www.designscopecompany.com/3dweave/
[43] ANSYS HFSS. *3D Full-Wave Electromagnetic Field Simulation*. Accessed: Nov. 20, 2018. [Online]. Available: http://www.ansoft.com/products/hf/hfss/
[44] Computer Simulation Technology. Accessed: Nov. 20, 2018. [Online]. Available: www.cst.com/
[45] M. Bozzi, A. Georgiadis, and K. Wu, "Review of substrate-integrated waveguide circuits and antennas," *IET Microw. Antennas Propag.*, vol. 5, no. 8, pp. 909–920, Jun. 2011.
[46] Z. Xu, L. Gardner, and A. J. Sadowski, "Nonlinear stability of elastic elliptical cylindrical shells under uniform bending," *Int. J. Mech. Sci.*, vols. 128–129, pp. 593–606, Aug. 2017.

LETICIA ALONSO-GONZÁLEZ (S'14–M'18) received the M.Sc. degree in telecommunications engineering from the University of Oviedo, Gijón, Spain, in 2014, the M.Sc. degree in systems and control engineering from the National University of Distance Learning and the Universidad Complutense de Madrid, Spain, in 2018, and the Ph.D. degree from the University of Oviedo, Spain, in 2018.

Since 2014, she has been a Researcher with the Signal Theory and Communications Group, University of Oviedo. She was a Visiting Scholar at the George Green Institute for Electromagnetics Research, University of Nottingham, U.K., in 2017. Her main research effort is focused on the design, simulation and manufacturing techniques to develop microwave and millimeter-wave passive circuits and antennas fully integrated in textile technology.

SAMUEL VER-HOEYE (M'05) received the M.Sc. degree in electronic engineering from the University of Gent, Gent, Belgium, in 1999, and the Ph.D. degree from the University of Cantabria, Santander, Spain, in 2002.

He is currently an Associate Professor with the Department of Electrical and Electronic Engineering, University of Oviedo, Gijón, Spain. His main research interests are focused on the design and analysis of nonlinear oscillator based circuits, millimeter wave and terahertz antennas, circuits and systems, graphene-based components, and textile integrated circuits and antennas.

MIGUEL FERNÁNDEZ-GARCÍA received the M.Sc. degree in telecommunication engineering, the M.Sc. degree in information technology and mobile communications, and the Ph.D. degree from the University of Oviedo, Gijón, Spain, in 2006, 2010, and 2010, respectively.

From 2006 to 2008, he was a Research Fellow with the Signal Theory and Communications Group, University of Oviedo, where he has been an Associate Professor since 2008. His current research interests include nonlinear analysis and optimization techniques for the design of oscillator-based circuits, active antennas and frequency multipliers and mixers at the microwave, millimeter/submillimeter-wave, and terahertz frequency bands.

CARLOS VÁZQUEZ-ANTUÑA received the M.Sc. degree in telecommunication engineering, the M.Sc. degree in information technology and mobile communications, and the Ph.D. degree from the University of Oviedo, Gijón, Spain, in 2007, 2008, and 2013, respectively.

From 2007 to 2012, he was a Graduate Research Assistant, and since 2012, he has been a Research Fellow with the Signal Theory and Communications Group, University of Oviedo. His research efforts mainly focus on nonlinear analysis and optimization techniques for the design of multifunctional oscillator-based circuits, active antennas, and passive components, such as frequency multipliers and harmonic mixers, at microwave, millimeter/submillimeter-wave, and terahertz frequencies.

FERNANDO LAS-HERAS ANDRÉS (M'86–SM'08) received the M.S. and Ph.D. degrees in telecommunication engineering from the Technical University of Madrid (UPM), Madrid, Spain, in 1987 and 1990, respectively.

He was a National Graduate Research Fellow, from 1988 to 1990, and an Associate Professor, from 1991 to 2000, with the Department of Signal, Systems and Radiocom, UPM. He was the Vice-Dean of Telecommunication Engineering with the Technical School of Engineering, Gijón, Spain, from 2004 to 2008. He was a Visiting Researcher with Syracuse University, New York, NY, USA, and a Visiting Lecturer with the National University of Engineering, Lima, Peru, and the École Supérieure d'Ingénieurs en Génie Électrique, Rouen, France. He has been the Head of the Signal Theory and Communications Research Group, Department of Electrical Engineering, University of Oviedo, Gijón, since 2001, and has been a Full Professor since 2003. He has authored over 450 technical journal and conference papers in the areas of electromagnetic radiation, propagation and scattering theory and applications as well as inverse problems.

Dr. Las-Heras Andrés held the Telefónica Chair on RF Technologies, ICTs Applied to Environment and Climate Change, and ICTs and Smartcities, from 2005 to 2015. He was a member of the Board of Directors of the IEEE Spain Section, from 2012 to 2015, and a member of the Science, Technology and Innovation Council of Asturias, Spain, in 2010. He is a member of the IEEE Microwaves and Antennas Propagation Chapter (AP03/MTT17) Board, from 2016 to 2018.